

Electron magnetic moment of chiral phonons

R. Matthias Geilhufe¹ and Wolfram Hergert²

¹*Department of Physics, Chalmers University of Technology, SE-412 96 Gothenburg, Sweden*

²*Institute of Physics, Martin Luther University Halle-Wittenberg, D-06120 Halle, Germany*

High intensity THz lasers allow for the coherent excitation of individual phonon modes. The ultrafast control of emergent magnetism by means of phonons opens up new tuning mechanisms for functional materials. While theoretically predicted phonon magnetic moments are tiny, recent experiments hint towards a significant magnetization in various materials. To explain these phenomena, we derive a coupling mechanism between the phonon angular momentum and the electron spin. This coupling introduces the transient level-splitting of spin-up and spin-down channels and a resulting magnetization. We estimate this magnetization on the example of the lowest infrared active mode in the perovskite KTaO_3 . Our results show an electronic magnetic moment of $\approx 0.2 \mu_B$ per unit cell, depending on the doping level and electron temperature.

Chiral phonons or circularly polarized phonons carry angular momentum [1, 2]. As the collective excitation of charged ions, a magnetization occurs. Such a magnetization can be understood in the framework of the dynamical multiferroicity [3], or, more specifically, the phonon inverse Faraday effect [4–7]. However, for a cyclotron motion, comparing the phonon magnetic moment $\mu_{\text{phonon}} = \frac{e\hbar}{2m_{\text{ion}}}$ with the electron magnetic moment $\mu_B = \frac{e\hbar}{2m_e}$, the effect is smaller by a factor of $\frac{m_{\text{ion}}}{m_e}$, i.e., in the range of the nuclear magneton [8, 9].

In contrast, recent experiments observed large phonon magnetic moments. In such experiments, optical phonons are excited with a circularly polarized THz laser pulse. Cheng *et al.* measured the phonon Zeeman effect in the Dirac semimetal Cd_3As_2 and observed a moment of $\approx 2.7 \mu_B$ [10]. They explain the giant magnetic moment by a coupling of the phonon to the effective Dirac electron, in resonance with the cyclotron frequency. Baydin *et al.* revealed a phonon Zeeman splitting of similar size in the semiconductor PbTe [11]. Here, the magnetic moment was explained in terms of strong anharmonicity effects. Basini *et al.* measured the dynamical magnetization by chiral phonons in SrTiO_3 using optical Kerr rotation, and, again found a magnetic moment of similar size [12]. They explained the effect by the angular momentum transfer from phonons to electrons in terms of the inverse Barnett effect and a resulting enhanced gyromagnetic ratio.

The mismatch of theory and experiment gives evidence that phonons cannot be described in the absence of electrons. Instead, electron-phonon and spin-phonon coupling play a significant role in explaining the emergent dynamical magnetization. One possible explanation was recently provided by Ren *et al.* [13], who showed that the second Chern form times the phonon angular momentum gives rise to a magnetization, in the framework of the modern theory of magnetization [14–16]. Here, we follow a different route in the framework of the spin-rotation coupling [17–20] and present estimates for a phonon induced dynamical magnetization in KTaO_3 in the pres-

ence of spin-phonon interaction.

For simplicity, we consider first a two-fold degenerate phonon mode $\mathbf{q} = (q_1, q_2)$ (in units $\text{\AA}\sqrt{u}$, with u the atomic mass unit) with eigenfrequency ω_0 . The phonon Lagrangian is given by [3]

$$\mathcal{L}^{\text{phonon}}(\mathbf{q}, \dot{\mathbf{q}}) = \frac{\dot{\mathbf{q}}^2}{2} - \frac{\omega_0^2 \mathbf{q}^2}{2}. \quad (1)$$

The electron Lagrangian of a non-relativistic electron in a nominally non-magnetic material and in the absence of external electromagnetic fields is given by

$$\begin{aligned} \mathcal{L}^{\text{electron}}(\Psi, \Psi^\dagger) \\ = \int d^3r \left[i\hbar \Psi^\dagger \dot{\Psi} - \Psi^\dagger \left(\frac{\hat{\mathbf{p}}^2}{2m} + V(\mathbf{r}) \right) \Psi \right]. \end{aligned} \quad (2)$$

We formulate the spin-phonon coupling term with symmetry arguments, by considering the two fundamental symmetries time-reversal \mathcal{T} and spatial inversion or parity \mathcal{P} . The phonon mode \mathbf{q} describes the displacement of ions from their equilibrium position. As a result, it transforms as a vector, being odd under \mathcal{P} and even under \mathcal{T} . It follows that the time-derivative $\dot{\mathbf{q}}$ is odd under both \mathcal{P} and \mathcal{T} . This is consistent with the transformation behavior of the phonon angular momentum $\mathbf{L}^{\text{phonon}} = \mathbf{q} \times \dot{\mathbf{q}}$, being a pseudo vector, i.e., even under \mathcal{P} and odd under \mathcal{T} . The same holds for the electron total angular momentum $\mathbf{J}^{\text{electron}} = \mathbf{L}^{\text{electron}} + \mathbf{S}^{\text{electron}}$, with $\mathbf{L}^{\text{electron}}$ being the orbital angular momentum and $\mathbf{S}^{\text{electron}}$ the spin. Hence, we can write down a \mathcal{P} and \mathcal{T} invariant scalar

$$\mathcal{L}^{\text{coupl.}} = -\alpha \mathbf{L}^{\text{phonon}} \cdot \langle \mathbf{J}^{\text{electron}} \rangle, \quad (3)$$

with α being a coupling constant in units of the inverse of the moment of inertia. Note, that we use a semi-classical approach here, with the phonon dynamics described classically. This is because we assume a non-equilibrium state with strong phonon amplitude. Hence, the phonon angular momentum is an actual angular momentum [21], as described towards the end of Ref. [22].

By expressing the phonon angular momentum in terms of the angular velocity ω^{phonon} and the moment of inertia I , equation (3) can be brought into the form of the spin-rotation coupling discussed in Ref. [17], $\mathcal{L}^{\text{coupl.}} = \omega^{\text{phonon}} \cdot \langle \mathbf{J}^{\text{electron}} \rangle = -I^{-1} \mathbf{L}^{\text{phonon}} \cdot \langle \mathbf{J}^{\text{electron}} \rangle$. The moment of inertia is given by $I = \int d\mathbf{r} r^2 m(\mathbf{r})$, with $m(\mathbf{r})$ the mass density.

Generally, the spin-phonon coupling emerges in rotating quantum systems [18–20, 23]. As assumed here, spin-rotation coupling becomes relevant for chiral phonons by the following argument. The spin rotation coupling is independent of the system size. Hence, first, we think of a system, rotating with frequency ω_1 , being shrunk to atomic length scale. In the second step, we add a second system, rotating with frequency ω_2 . If both systems are brought in close vicinity, a hopping of electrons between them is allowed. As a result, the energy levels of the coupled system, depend on the local rotations of the two individual systems. Extending the two-site model to a periodic lattice, the local rotations can be recast in terms of a chiral phonon. Note, however, that the ions precess about their equilibrium positions.

We extend our formalism, and continue by evaluating the chiral spin-phonon coupling (3) on the example of KTaO_3 . For the phonon degrees of freedom, we applied density functional theory following Ref. [8]. KTaO_3 is cubic with a lattice constant of 3.988 \AA [24]. We used the Vienna ab initio simulation package VASP [25] to calculate the dynamical matrix using i) a $2 \times 2 \times 2$ supercell; ii) density functional perturbation theory [26, 27]. The exchange correlation functional was approximated by the PBE generalized gradient approximation [28]. We used a \mathbf{k} -mesh density of $\approx 1050 \mathbf{k}$ -points/ \AA^{-3} , i.e., an $8 \times 8 \times 8$ mesh and a cut-off energy of 700 eV. The full phonon spectrum was calculated using Phonopy [29] and is shown in Fig. 1(a). The lowest calculated infrared active mode is three-fold degenerate and has a frequency of $f_0 = 3.05 \text{ THz}$. In experiments, this mode is observed to be strongly temperature dependent, taking values from $\approx 1 \text{ THz}$ at low temperatures (20 K) to values of $\approx 2.6 \text{ THz}$ at room temperature [30].

One corresponding Eigenmode with respect to the crystal structure Fig. 1(b) is shown in Fig. 1(c). The other two Eigenmodes are obtained by applying cubic symmetries. We first describe the phonon dynamics in the absence of electronic damping ($\mathcal{L}^{\text{coupl.}}$) and formulate a classical equation of motion [3, 8, 9, 12, 31, 32],

$$\ddot{u}_{i\alpha}(t) + \eta \dot{u}_{i\alpha}(t) + \sum_{j\beta} K_{i\alpha j\beta} u_{j\beta}(t) = \frac{Z_i}{m_i} E_{\alpha}^*(t) \quad (4)$$

Instead of the diagonal basis in terms of the phonon mode \mathbf{q} , we define the displacement \mathbf{u}_i per site i and denote the corresponding charge and mass by Z_i and m_i , respectively. This allows us to obtain a site-resolved phonon

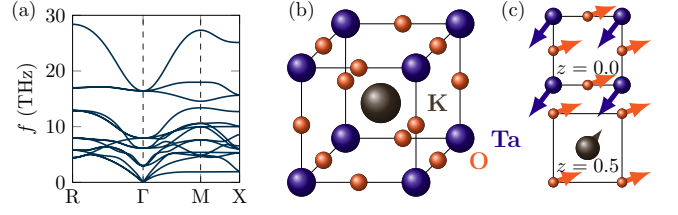


FIG. 1. Phonons in KTaO_3 . (a) Full phonon spectrum; (b) crystal structure; (c) eigenvector of the lowest infrared active mode with the computational value of $f_0 \approx 3.05 \text{ THz}$.

angular momentum, which, in the next step, we couple to the corresponding electronic orbitals. \mathbf{K} is the dynamical matrix and η the empirical damping factor. All material parameters are summarized in Tab. I. The electric field within the medium \mathbf{E}^* is screened and related to the vacuum electric field \mathbf{E} by $\mathbf{E}^* = \epsilon^{-1} \mathbf{E}$. Due to cubic symmetry, the dielectric tensor is diagonal, with $\epsilon_{ii} = \epsilon_{\infty} = 5.4$ [8], which is slightly larger than the experimentally observed value of $\epsilon_{\infty} = 4.3$ [33].

The numerical solution of equation (4) for a Gaussian laser pulse with a 2 ps pulse width, amplitude of 1 MVcm^{-1} , and frequency 3.05 THz is shown in Fig. 2. Lacking experimental values for the phonon lifetime, we assume a heuristic value of $\eta = 0.1 \times 2\pi \text{ THz}$, leading to a phonon lifetime of $\approx 10 \text{ ps}$. We focus on O and Ta, as they are the relevant atoms in the electronic structure discussed below. The largest displacement from the atomic equilibrium position is $\approx 4 \text{ pm}$. The peak in the site-resolve phonon angular momentum occurs $\approx 1 \text{ ps}$ after the maximal amplitude of the laser pulse and reaches values of $0.8 \hbar$ ($0.05 \hbar$) for Ta (O). 1 ps later, when the laser pulse has fully decayed, the phonon angular momentum of Ta is still considerable, i.e., $0.4 \hbar$. Hence, a phonon induced magnetization can be probed when the laser is fully decayed which allows disentangling the effect from e.g., the inverse Faraday effect. To remind the reader, the inverse Faraday effect is the emergence of a DC magnetization of a sample, exposed to circularly polarized light. It originates from the time-reversal symmetry breaking due to the photon angular momentum, a term which couples to the magnetic field in the free energy [34]. In contrast, the phonon inverse Faraday effect emerges due to circularly polarized phonons and does not require the presence of an external electric field. Instead a magnetization is also predicted for thermally excited chiral phonons [35–37].

	K	Ta	O
mass [u]	39.1	180.95	16.0
charge Z_i [e]	0.867	4.954	-1.940

TABLE I. DFT calculated site parameters.

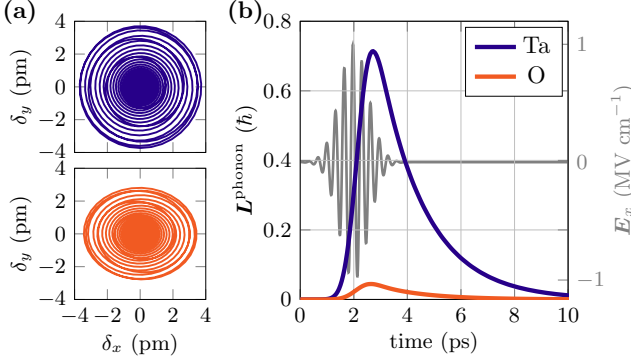


FIG. 2. Calculated atomic motion of oxygen and tantalum in the damped circularly polarized phonon excitation. (a) Displacement δ ; (b) site-resolved phonon angular momentum and laser pulse in resonance with the lowest infrared active mode of KTaO₃. The damping is $\eta = 0.1 \times 2\pi$ THz.

From the phonon angular momentum, the ionic contribution to an emergent magnetization is estimated from $\mathbf{M}_i^{\text{phonon}} = \gamma \mathbf{L}_i^{\text{phonon}}$, with $\gamma = \frac{Z_i}{2m_i}$. Taking the bare charge and mass of Ta given in Tab. I, we obtain $|\mathbf{M}|_{\text{Ta}} \approx 2.2 \times 10^{-2} \mu_N \approx 1.2 \times 10^{-5} \mu_B$. We continue by estimating the electronic contribution to the phonon induced magnetization.

The electronic structure of KTaO₃ is modeled in a two-center Slater-Koster tight-binding scheme [38, 39] as implemented in the Mathematica group theory package GT-Pack [40, 41] (cf. Appendix). The band structure close to the Fermi energy is plotted in Fig. 3(a). The valence bands are mainly composed of the O-*p* orbitals, whereas the conduction band is dominated by contributions from Ta-*d* orbitals. The splitting into *t*_{2g} and *e*_g bands due to cubic symmetry is clearly revealed. The band gap is ≈ 2.8 eV and lower than the experimentally observed optical band gap of ≈ 3.6 eV [42]. The splitting of the *t*_{2g} band at Γ due to spin-orbit interaction is ≈ 0.46 eV.

In the presence of transient chiral phonons, the time-reversal symmetry of the system is broken. As a result, Kramers degeneracy of the electronic bands is lifted. To model this scenario, the tight-binding Hamiltonian is extended by the spin-phonon coupling of equation (3). We choose $I^{-1} \mathbf{L}^{\text{phonon}} = \boldsymbol{\omega}$ [17], with $\boldsymbol{\omega}$ being the angular velocity of the site-resolved displacement having the frequency $\omega_0 = 3.05 \times 2\pi$ THz. The corresponding coupling to the total angular momentum of the electron, $\boldsymbol{\omega} \cdot \mathbf{J}$ is diagonal in the $|j, \mu\rangle$ basis. We project the resulting band structure onto spin-up and spin-down channels as shown in Fig. 3(b). We calculate the emergent magnetization by

$$M_z = \mu_B (N_{\uparrow} - N_{\downarrow}), \quad N_{\sigma} = \int_{-\infty}^{\infty} dE n_{\sigma}(E) f(E, \mu, T), \quad (5)$$

with $n_{\sigma}(E)$ the electronic density of states of spin σ and

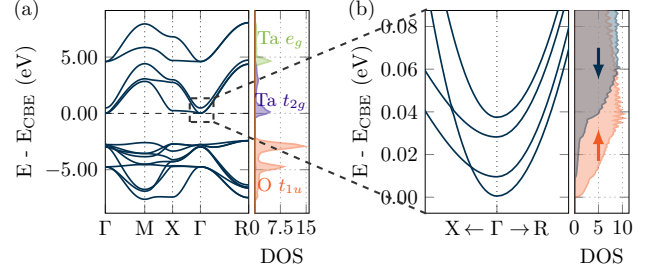


FIG. 3. Electronic structure of KTaO₃ relative to the conduction band edge (E_{CBE}). (a) Full band structure. (b) Expected band splitting of the conduction band due to spin-rotation coupling close to the Γ point. The DOS is projected on spin-up and spin-down channels.

$f(E, \mu, T)$ the Fermi-Dirac distribution.

The magnetization (5) is computed with the tight-binding band structure in Fig. 3(b). The dynamically induced magnetization is shown in dependence of the chemical potential μ and electron temperature T in Fig. 4. As can be seen, an electronic magnetization of $\approx 0.2 \mu_B$ can be achieved.

In the estimates, we focus on the chemical potential close to the conduction band edge. In fact, intrinsic doping in KTaO₃ crystals, e.g., due to O-vacancies induce sub-gap states originating from *d*-electrons of Ta atoms close to the O vacancy [43, 44]. While a natural amount of doping ($< 10^{18}$ charge carriers/cm³) still leads to an insulating behavior, a larger amount of O vacancies can induce a metallic state [45]. In the insulating state, a fairly large magnetization occurs if the electronic temperature becomes high. Such a situation might occur for short durations after the crystal was exposed to the laser light [46, 47]. Due to the reduced mass of electrons compared to ions, the kinetic energy will be significantly larger until it relaxes into an equilibrium state together with the ions. In contrast, if the Fermi level slightly cuts the conduction band, a lower electronic temperature would be required to exclude contributions to the magnetization from the minority spin-channel. Also, we note that electrons can be excited from the sub-gap states into the conduction band by a multiphoton process in intense laser fields. Specifically, for low photon energy THz fields, the photon density is significantly higher, making a multi-photon process more likely. Also, such a mechanism can lead to the formation of excitons and induce the transient shift of the chemical potential for electrons and holes.

In summary, we discussed the effect of the chiral spin-phonon coupling $\sim \mathbf{L}^{\text{phonon}} \cdot \mathbf{J}^{\text{electron}}$ which occurs after excitation of chiral phonons. This mechanism induces a split of electronic spin states in the adiabatic approximation. As a consequence, a mismatch of occupied spin-up and spin-down states leads to an emergent magnetiza-

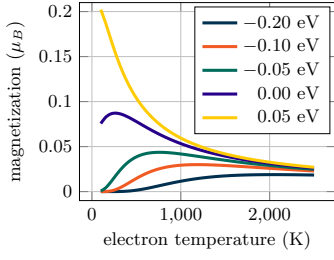


FIG. 4. Electronic magnetization due to spin-phonon interaction. Estimates are given for various values of the chemical potential, relative to the conduction band minimum.

tion in the order of $10^{-1} \mu_B$. Hence, the effect is larger than the purely ionic phonon inverse Faraday effect by 3-4 orders of magnitude. The chiral spin-phonon coupling might be relevant to explain the large experimentally observed phonon magnetic moments due to chiral phonons in various materials [10–12]. Furthermore, also the opposite effect, i.e., the transfer of electronic angular momentum to the lattice can be described by the chiral spin-phonon coupling and would contribute, e.g., to ultrafast demagnetization effects [21, 48, 49]. The chiral spin-phonon coupling term discussed here is different to previously reported spin-phonon coupling terms, where, e.g., phonons couple to spin indirectly through spin-orbit interaction [50–52], via magnetic exchange [53, 54], or an inverse Katsura-Nagaosa-Balatsky mechanism [55–57]. Finally, we note that in a recent paper, Li *et al.* [37] described the generation of a chiral phonon activated spin Seebeck effect, where the spin couples to a temperature gradient and resulting chiral phonons. We assume that the corresponding coupling constant is related to the mechanism described here.

Acknowledgment. We are grateful for inspiring discussions with A. V. Balatsky, S. Bonetti, M. Basini, D. Juraschek, G. Fiete, M. Rodriguez-Vega, and A. Ernst. RMG acknowledges support from Chalmers University of Technology. Computational resources were provided by the Swedish National Infrastructure for Computing (SNIC) via the High Performance Computing Centre North (HPC2N) and the Uppsala Multidisciplinary Centre for Advanced Computational Science (UPPMAX).

APPENDIX

We construct the tight-binding Hamiltonian using the Slater-Koster scheme [38, 39] as implemented in the Mathematica group theory package GTPack [40, 41]. A restricted basis set containing O p -orbitals and Ta d -orbitals is used. Spin-orbit coupling of Ta d -orbitals is included. The Hamiltonian in two-center approximation considers nearest neighbor interactions of Ta and nearest and next-nearest neighbor interactions of O. The Hamil-

tonian is represented by a 28×28 matrix and contains 14 parameters (s. Tab. II). The crystal field splitting for the on-site parameters is taken into account.

TABLE II. Tight-binding parameters of the Hamiltonian

$(dd\sigma)_1^{\text{Ta,Ta}}$	$(dd\pi)_1^{\text{Ta,Ta}}$	$(dd\delta)_1^{\text{Ta,Ta}}$	$(pp\sigma)_1^{\text{O,O}}$	$(pp\pi)_1^{\text{O,O}}$	$(pp\sigma)_2^{\text{O,O}}$	$(pp\pi)_2^{\text{O,O}}$
0.11409	-0.24820	0.02087	0.38702	-0.0955	0.14458	-0.042634
$(pd\sigma)_1^{\text{O,Ta}}$	$(pd\pi)_1^{\text{O,Ta}}$	$(dd0)_{t2g}^{\text{Ta}}$	$(dd0)_{eg}^{\text{Ta}}$	$(pp0)_\perp^{\text{O}}$	$(pp0)_\parallel^{\text{O}}$	ξ
-2.77242	1.57614	3.08778	6.15932	-1.4078	-2.44059	0.28868

The tight-binding Hamiltonian is fitted to DFT band structure data (computational details given in the main text). We refine an initial guess by the least squares method. 15 \mathbf{k} -points are taken along each symmetry line. To avoid the algorithm getting stuck in a local minimum in parameter space, we add noise to the parameters after a first step and repeat the minimization scheme. The final result is shown in Fig. 5. It can be seen that the relevant conduction band is well-parametrized close to the Γ point.

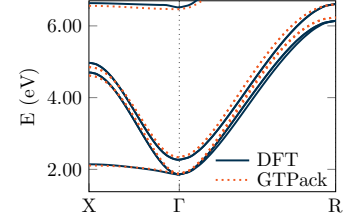


FIG. 5. Comparison of the DFT band structure and the 2-center tight-binding band structure using GTPack.

- [1] L. Zhang and Q. Niu, Angular momentum of phonons and the Einstein–de Haas effect, *Physical Review Letters* **112**, 085503 (2014).
- [2] A. McLellan, Angular momentum states for phonons and a rotationally invariant development of lattice dynamics, *Journal of Physics C: Solid State Physics* **21**, 1177 (1988).
- [3] D. M. Juraschek, M. Fechner, A. V. Balatsky, and N. A. Spaldin, Dynamical multiferroicity, *Physical Review Materials* **1**, 014401 (2017).
- [4] D. M. Juraschek, T. c. v. Neuman, and P. Narang, Giant effective magnetic fields from optically driven chiral phonons in $4f$ paramagnets, *Physical Review Research* **4**, 013129 (2022).
- [5] D. M. Juraschek, D. S. Wang, and P. Narang, Sum-frequency excitation of coherent magnons, *Physical Review B* **103**, 094407 (2021).
- [6] D. M. Juraschek, P. Narang, and N. A. Spaldin, Phonomagnetic analogs to opto-magnetic effects, *Physical Review Research* **2**, 043035 (2020).
- [7] Y. T. Rebane, Faraday effect produced in the residual ray region by the magnetic moment of an optical phonon in an ionic crystal, *Journal of Experimental and Theoretical Physics* **84**, 2323 (1983).

- [8] R. M. Geilhufe, V. Juričić, S. Bonetti, J.-X. Zhu, and A. V. Balatsky, Dynamically induced magnetism in ktao 3, *Physical Review Research* **3**, L022011 (2021).
- [9] D. M. Juraschek and N. A. Spaldin, Orbital magnetic moments of phonons, *Physical Review Materials* **3**, 064405 (2019).
- [10] B. Cheng, T. Schumann, Y. Wang, X. Zhang, D. Barbalas, S. Stemmer, and N. Armitage, A large effective phonon magnetic moment in a dirac semimetal, *Nano Letters* **20**, 5991 (2020).
- [11] A. Baydin, F. G. G. Hernandez, M. Rodriguez-Vega, A. K. Okazaki, F. Tay, G. T. Noe, I. Katayama, J. Takeda, H. Nojiri, P. H. O. Rappl, E. Abramof, G. A. Fiete, and J. Kono, Magnetic control of soft chiral phonons in pbte, *Physical Review Letters* **128**, 075901 (2022).
- [12] M. Basini, M. Pancaldi, B. Wehinger, T. Terumasa, M. C. Hoffmann, A. V. Balatsky, and S. Bonetti, Terahertz electric-field driven magnetism in a perovskite, in progress.
- [13] Y. Ren, C. Xiao, D. Saparov, and Q. Niu, Phonon magnetic moment from electronic topological magnetization, *Physical Review Letters* **127**, 186403 (2021).
- [14] D. Xiao, J. Shi, and Q. Niu, Berry phase correction to electron density of states in solids, *Physical Review Letters* **95**, 137204 (2005).
- [15] T. Thonhauser, D. Ceresoli, D. Vanderbilt, and R. Resta, Orbital magnetization in periodic insulators, *Physical Review Letters* **95**, 137205 (2005).
- [16] R. Resta, Electrical polarization and orbital magnetization: the modern theories, *Journal of Physics: Condensed Matter* **22**, 123201 (2010).
- [17] R. M. Geilhufe, Dynamic electron-phonon and spin-phonon interactions due to inertia, *Physical Review Research* **4**, L012004 (2022).
- [18] M. Matsuo, J. Ieda, K. Harii, E. Saitoh, and S. Maekawa, Mechanical generation of spin current by spin-rotation coupling, *Physical Review B* **87**, 180402 (2013).
- [19] M. Matsuo, J. Ieda, E. Saitoh, and S. Maekawa, Effects of mechanical rotation on spin currents, *Physical Review Letters* **106**, 076601 (2011).
- [20] M. Matsuo, J. Ieda, E. Saitoh, and S. Maekawa, Spin-dependent inertial force and spin current in accelerating systems, *Physical Review B* **84**, 104410 (2011).
- [21] S. R. Tauchert, M. Volkov, D. Ehberger, D. Kazenwadel, M. Evers, H. Lange, A. Donges, A. Book, W. Kreuzpaintner, U. Nowak, *et al.*, Polarized phonons carry angular momentum in ultrafast demagnetization, *Nature* **602**, 73 (2022).
- [22] S. Streib, Difference between angular momentum and pseudoangular momentum, *Physical Review B* **103**, L100409 (2021).
- [23] F. W. Hehl and W.-T. Ni, Inertial effects of a dirac particle, *Physical Review D* **42**, 2045 (1990).
- [24] E. A. Zhurova, Y. Ivanov, V. Zavodnik, and V. Tsirelson, Electron density and atomic displacements in ktao_3 , *Acta Crystallographica Section B: Structural Science* **56**, 594 (2000).
- [25] G. Kresse and J. Furthmüller, Efficient iterative schemes for ab initio total-energy calculations using a plane-wave basis set, *Physical Review B* **54**, 11169 (1996).
- [26] R. D. King-Smith and D. Vanderbilt, Theory of polarization of crystalline solids, *Physical Review B* **47**, 1651 (1993).
- [27] M. Gajdoš, K. Hummer, G. Kresse, J. Furthmüller, and F. Bechstedt, Linear optical properties in the projector-augmented wave methodology, *Physical Review B* **73**, 045112 (2006).
- [28] J. P. Perdew, K. Burke, and M. Ernzerhof, Generalized gradient approximation made simple, *Physical review letters* **77**, 3865 (1996).
- [29] A. Togo and I. Tanaka, First principles phonon calculations in materials science, *Scripta Materialia* **108**, 1 (2015).
- [30] C. H. Perry, R. Currat, H. Buhay, R. M. Migoni, W. G. Stirling, and J. D. Axe, Phonon dispersion and lattice dynamics of KTaO_3 from 4 to 1220 K, *Physical Review B* **39**, 8666 (1989).
- [31] M. Kozina, M. Fechner, P. Marsik, T. van Driel, J. M. Glowina, C. Bernhard, M. Radovic, D. Zhu, S. Bonetti, U. Staub, *et al.*, Terahertz-driven phonon upconversion in SrTiO_3 , *Nature Physics* **15**, 387 (2019).
- [32] A. Cartella, T. F. Nova, M. Fechner, R. Merlin, and A. Cavalleri, Parametric amplification of optical phonons, *Proceedings of the National Academy of Sciences* **115**, 12148 (2018).
- [33] A. S. Barker and J. J. Hopfield, Coupled-optical-phonon-mode theory of the infrared dispersion in BaTiO_3 , SrTiO_3 , and KTaO_3 , *Physical Review* **135**, A1732 (1964).
- [34] P. Pershan, J. Van der Ziel, and L. Malmstrom, Theoretical discussion of the inverse faraday effect, raman scattering, and related phenomena, *Physical review* **143**, 574 (1966).
- [35] M. Hamada and S. Murakami, Conversion between electron spin and microscopic atomic rotation, *Physical Review Research* **2**, 023275 (2020).
- [36] I. G. Gurtubay, A. Iturbe-Beristain, and A. Eiguren, Magnetic oscillations induced by phonons in non-magnetic materials, *Communications Physics* **3**, 1 (2020).
- [37] X. Li, J. Cheng, L. Zhang, and J. Zhou, Chiral phonon activated spin seebeck effect, *arXiv:2105.08485* (2021).
- [38] A. V. Podolskiy and P. Vogl, Compact expression for the angular dependence of tight-binding hamiltonian matrix elements, *Physical Review B* **69**, 233101 (2004).
- [39] J. C. Slater and G. F. Koster, Simplified lcao method for the periodic potential problem, *Physical Review* **94**, 1498 (1954).
- [40] R. M. Geilhufe and W. Hergert, GTPack: A Mathematica Group Theory Package for Application in Solid-State Physics and Photonics, *Frontiers in Physics* **6**, 86 (2018).
- [41] W. Hergert and R. M. Geilhufe, *Group Theory in Solid State Physics and Photonics: Problem Solving with Mathematica* (Wiley-VCH, 2018) ISBN: 978-3-527-41133-7.
- [42] G. E. Jellison, I. Paulauskas, L. A. Boatner, and D. J. Singh, Optical functions of ktao_3 as determined by spectroscopic ellipsometry and comparison with band structure calculations, *Physical Review B* **74**, 155130 (2006).
- [43] M. Choi, F. Oba, and I. Tanaka, Hybrid density functional study of oxygen vacancies in ktao_3 and natao_3 , *Physical Review B* **83**, 214107 (2011).
- [44] P. Modak and B. Modak, Energetic, electronic, and optical properties of intrinsic charge carrier-trapping defects in ktao_3 : Insights from a hybrid dft study, *The Journal of Physical Chemistry C* **125**, 24067 (2021).
- [45] K. Ueno, S. Nakamura, H. Shimotani, H. Yuan, N. Kimura, T. Nojima, H. Aoki, Y. Iwasa, and

- M. Kawasaki, Discovery of superconductivity in KtAO_3 by electrostatic carrier doping, *Nature nanotechnology* **6**, 408 (2011).
- [46] L. Alber, V. Scalera, V. Unikandanunni, D. Schick, and S. Bonetti, Nttmpy: An open source package for solving coupled parabolic differential equations in the framework of the three-temperature model, *Computer Physics Communications* **265**, 107990 (2021).
- [47] V. Unikandanunni, F. Rigoni, M. C. Hoffmann, P. Vavassori, S. Urazhdin, and S. Bonetti, Ultrafast electron dynamics in platinum and gold thin films driven by optical and terahertz fields, *Applied Physics Letters* **120**, 021601 (2022).
- [48] T. Tsatsoulis, C. Illg, M. Haag, B. Y. Mueller, L. Zhang, and M. Fähnle, Ultrafast demagnetization after femtosecond laser pulses: Transfer of angular momentum from the electronic system to magnetoelastic spin-phonon modes, *Physical Review B* **93**, 134411 (2016).
- [49] B. Koopmans, G. Malinowski, F. Dalla Longa, D. Steiauf, M. Fähnle, T. Roth, M. Cinchetti, and M. Aeschliemann, Explaining the paradoxical diversity of ultrafast laser-induced demagnetization, *Nature materials* **9**, 259 (2010).
- [50] R. J. Elliott, Theory of the effect of spin-orbit coupling on magnetic resonance in some semiconductors, *Physical Review* **96**, 266 (1954).
- [51] Y. Yafet, *Solid state physics*. vol. 14/edited by f. seitz and d. turnbull (1963).
- [52] C. Illg, M. Haag, and M. Fähnle, Ultrafast demagnetization after laser irradiation in transition metals: Ab initio calculations of the spin-flip electron-phonon scattering with reduced exchange splitting, *Physical Review B* **88**, 214404 (2013).
- [53] J. Son, B. C. Park, C. H. Kim, H. Cho, S. Y. Kim, L. J. Sandilands, C. Sohn, J.-G. Park, S. J. Moon, and T. W. Noh, Unconventional spin-phonon coupling via the dzyaloshinskii-moriya interaction, *npj Quantum materials* **4**, 1 (2019).
- [54] M. C. Weber, M. Guennou, D. M. Evans, C. Toulouse, A. Simonov, Y. Kholina, X. Ma, W. Ren, S. Cao, M. A. Carpenter, *et al.*, Emerging spin-phonon coupling through cross-talk of two magnetic sublattices, *Nature Communications* **13**, 1 (2022).
- [55] H. Katsura, N. Nagaosa, and A. V. Balatsky, Spin current and magnetoelectric effect in noncollinear magnets, *Physical Review Letters* **95**, 057205 (2005).
- [56] M. Mostovoy, Ferroelectricity in spiral magnets, *Physical Review Letters* **96**, 067601 (2006).
- [57] M. Mochizuki, N. Furukawa, and N. Nagaosa, Theory of spin-phonon coupling in multiferroic manganese perovskites RmnO_3 , *Physical Review B* **84**, 144409 (2011).